Influence of Coupling Capacitor Voltage Transformers on Travelling Wave-Based Fault Locators

R. L. A. Reis, F. V. Lopes, W. L. A. Neves and D. Fernandes Jr.

***Abstract*-- The coupling capacitor voltage transformer (CCVT) performance is quite acceptable during steady-state, but it is far from ideal when the power system is subjected to short-circuits conditions. In this paper, the influence of two 230 kV and one 500 kV CCVT on a two-terminal travelling wave-based fault location algorithm is analyzed, when only voltage measurements are available. Several fault scenarios were simulated using the Alternative Transients Program (ATP). In each case, the fault location was estimated using two-terminal synchronized voltage samples taken from the primary and secondary terminals of the modeled CCVTs. To provide a more thorough study, two different transient detection methods available in the literature were used to implement the analyzed fault location method. The obtained results indicate that the estimated fault locations are directly affected by the CCVT frequency response.**

***Keywords*: CCVT, travelling waves, fault location, electromagnetic transients, transient detection.**

I. Introduction

THE Coupling Capacitor Voltage Transformer is the predominant equipment for voltage signal measurement in High Voltage (HV) and Extra High Voltage (EHV) systems, since it provides a cost-efficient way of obtaining secondary voltages [1]. Therefore, CCVTs are of great importance for protection and control systems that depend on the analysis of voltage waveform samples.

The electrical power system protection is primarily performed by digital relays. The proper and safe functioning of the power system depends on the reliable operation of the relays, which in turn are subject to errors inherent to the instrument transformers, such as Current Transformers (CT) and CCVTs [2].

During the steady state, the CCVT secondary voltage waveform is almost an ideal replica of the primary voltage at power frequency, which has an acceptable accuracy for most protection applications. However, during faults on transmission lines, when the primary voltage collapses, the CCVT secondary voltage may be quite different from the voltage waveform at the primary side. This phenomenon is due to the energy stored in the stack capacitors and the tuning reactor of the CCVT's electric circuit, which need to be dissipated. As a consequence, since voltages across the capacitors and currents through the reactors cannot vary instantaneously, undesirable wave shapes appear in secondary side [1], [2], which can lead to malfunctioning or substantial delay in the tripping process of protective devices and jeopardize the fault-location process as well [3]. In this context, great efforts have been taken towards reducing the CCVT-induced transient errors on the operation of both relaying and fault-location algorithms [2], [4], [5], [6].

In the literature, there are several references indicating the negative influence of the CCVT transient behavior on the performance of protection algorithms [1], [3], [4], control techniques, measurement of harmonics and fault location methods. Transmission line fault location errors due to a 230 kV CCVT type using a travelling wave-based method was reported in [5].

Here a thorough investigation is carried out for two 230 kV and one 500 kV CCVT models obtained from the open literature for situations in which only voltage waveform samples are available. To detect fault-induced transients, methods based on Park's Transformation (TDQ) [7] and Maximal Overlap Discrete Wavelet Transform (MODWT) [8] were used.

The proposed analysis is carried out through ATP simulations of faults on power systems with rated voltages of 230 kV and 500 kV. In each case, voltage samples from the CCVT`s primary and secondary sides were taken as inputs of the fault-induced transient methods in order to analyze the CCVT influence on travelling wave-based fault locators.

II. The Analyzed CCVTs

The two 230 kV CCVTs are named CCVT 1 [9], and CCVT 2 [10], and the 500 kV CCVT is named CCVT 3 [6]. The required circuit topology and data parameters are shown in Fig. 1 and Table I, respectively. The CCVT responses are the same for fundamental frequency. However, since they have different electrical circuits, their frequency response are quite distinct, specially in the high frequency spectrum, leading them

This work was supported by the Brazilian Coordination for the Improvement of Higher Education Personnel (CAPES).

R. L. A. Reis is with the Department of Electrical Engineering of Federal University of Campina Grande (UFCG), 58429-900 Campina Grande, Paraíba, Brazil (e-mail: raphael.reis@ee.ufcg.edu.br).

F. V. Lopes is with the Department of Electrical Engineering at University of Brasília (UnB), (e-mail: felipevlopes@unb.br).

W. L. A. Neves and D. Fernandes Jr. are with the Department of Electrical Engineering of Federal University of Campina Grande (UFCG) (e-mail: waneves@dee.ufcg.edu.br and damasio@dee.ufcg.edu.br).

Paper submitted to the International Conference on Power Systems Transients (IPST2015) in Cavtat, Croatia June 15-18, 2015

to present different dynamic behavior whenever the power system is subject to voltage transients. The ATP FREQUENCY SCAN routine [11] was used for a frequency range from 1 Hz to 100 kHz. It produces the magnitude and angle frequency response plot for CCVT 1, CCVT 2 and CCVT 3 shown in Figs. 2, 3, and 4, respectively.

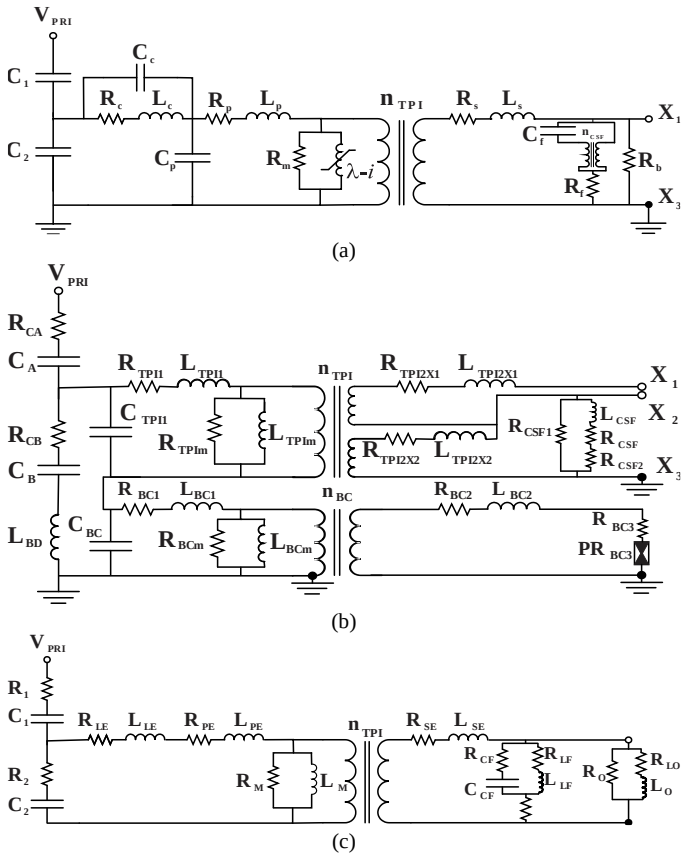

Fig. 1. The CCVT's equivalent circuits: (a) CCVT 1; (b) CCVT 2; (c) CCVT 3.

TABLE I
THE CCVT'S PARAMETERS

CCVT 1		CCVT 2		CCVT 3	
Parameter	Value	Parameter	Value	Parameter	Value
C_1 (nF)	2.43	C_A (pF)	4321	C_1 (nF)	1.605
C_2 (nF)	82	C_B (pF)	38820	C_2 (nF)	89.991
C_c (pF)	100	C_{TPI1} (pF)	200	C_f (μF)	165.36
C_p (pF)	150	C_{BC} (pF)	1500	L_{LE} (H)	67.922
C_f (μF)	9.6	L_{TPI1} (H)	6.93	L_f (mH)	54.3
L_c (H)	153.85	L_{TPI2X1} (mH)	0.0268	L_{PE} (H)	4.4433
L_p (H)	7.95	L_{TPI2X2} (mH)	0.0368	L_{SE} (μH)	649.91
L_s (μH)	2.653	L_{BC1} (H)	1.32	L_O (H)	0.0982
R_c (Ω)	228	L_{BC2} (mH)	3.56	R_1 (Ω)	3310.7
R_p (Ω)	400	L_{BD} (mH)	45	R_2 (Ω)	59.0338
R_s (Ω)	0.001	R_{CA} (Ω)	1565	R_{LE} (Ω)	950.06
R_f (Ω)	40	R_{CB} (Ω)	177.6	R_F (Ω)	13.333
R_b (Ω)	100	R_{TPI1} (Ω)	343	R_{CF} (Ω)	0.08
n_{CSF}	1.98	R_{TPI2X1} (mΩ)	8.6	R_{LF} (Ω)	1.2301
n_{TPI} ($X_1 - X_3$)	57.25	R_{TPI2X2} (mΩ)	11.8	R_{PE} (Ω)	850.02
λ (V.s)	13,7867	R_{BC1} (Ω)	382	R_{SE} (Ω)	0.2467
i (mA)	1,421	R_{BC2} (Ω)	5.64	R_O (Ω)	29.551
		R_{BC3} (Ω)	24.8	R_{LO} (Ω)	0
		R_{CSF} (Ω)	1.33	n_{TPI}	75.8503
		R_{CSF1} (Ω)	74.6		
		R_{CSF2} (Ω)	2.1		
		R_{TPIm} (MΩ)	11.2		
		R_{BC} (MΩ)	1.26		
		n_{TPI} ($X_1 - X_3$)	116.13		
		n_{TPI} ($X_2 - X_3$)	201.1		
		n_{BC}	19.23		

With the purpose of making possible a comparative analysis among the obtained frequency responses and the ideal one taken from the primary circuit (in this work, the primary voltage signal is taken as reference), all voltage magnitude frequency responses were normalized in per unit values. The angle responses are shown in degrees.

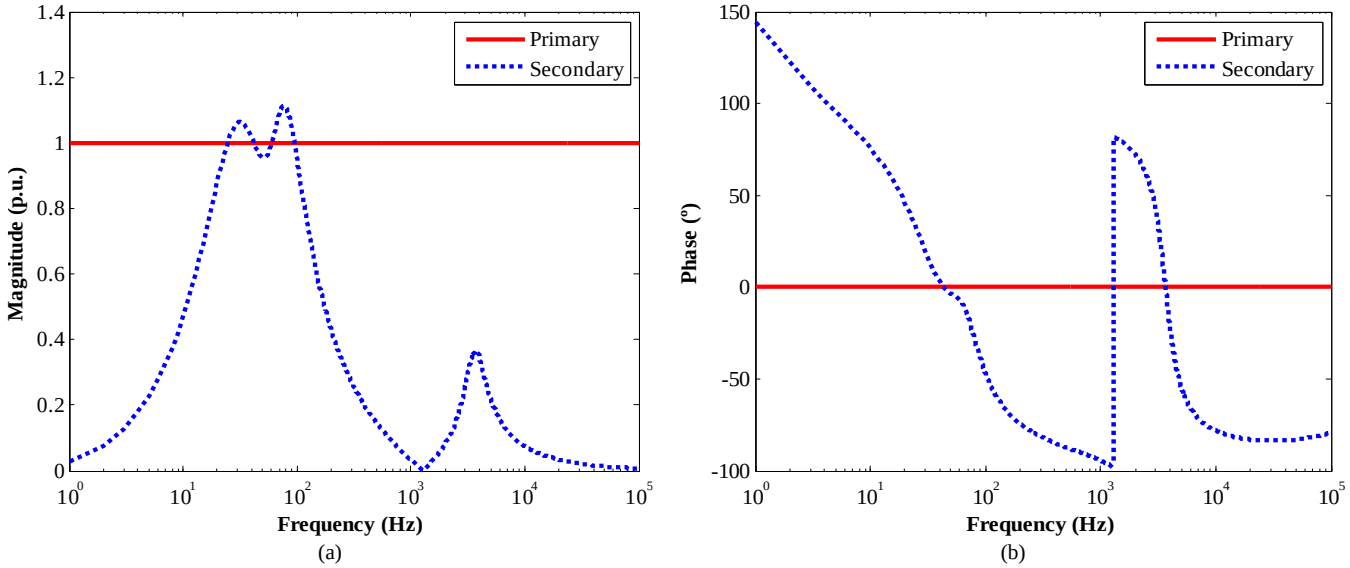

Fig. 2. CCVT 1 Frequency response: (a) Magnitude (p.u.); (b) phase (°).

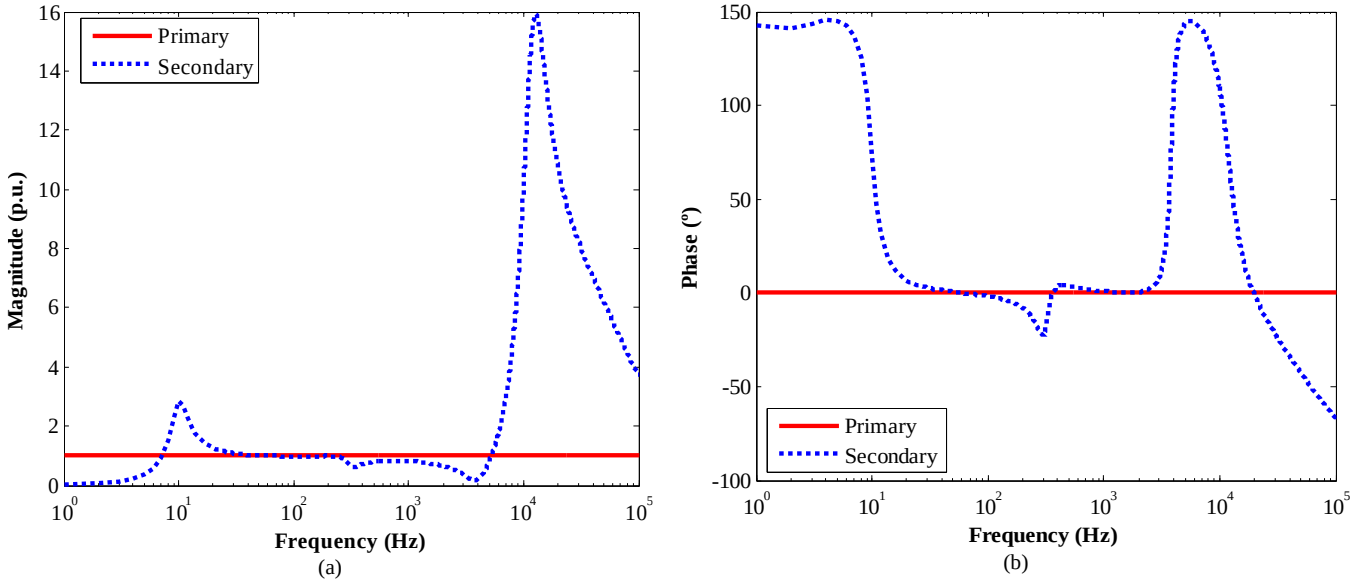

Fig. 3. CCVT 2 Frequency response: (a) Magnitude (p.u.); (b) phase (°).

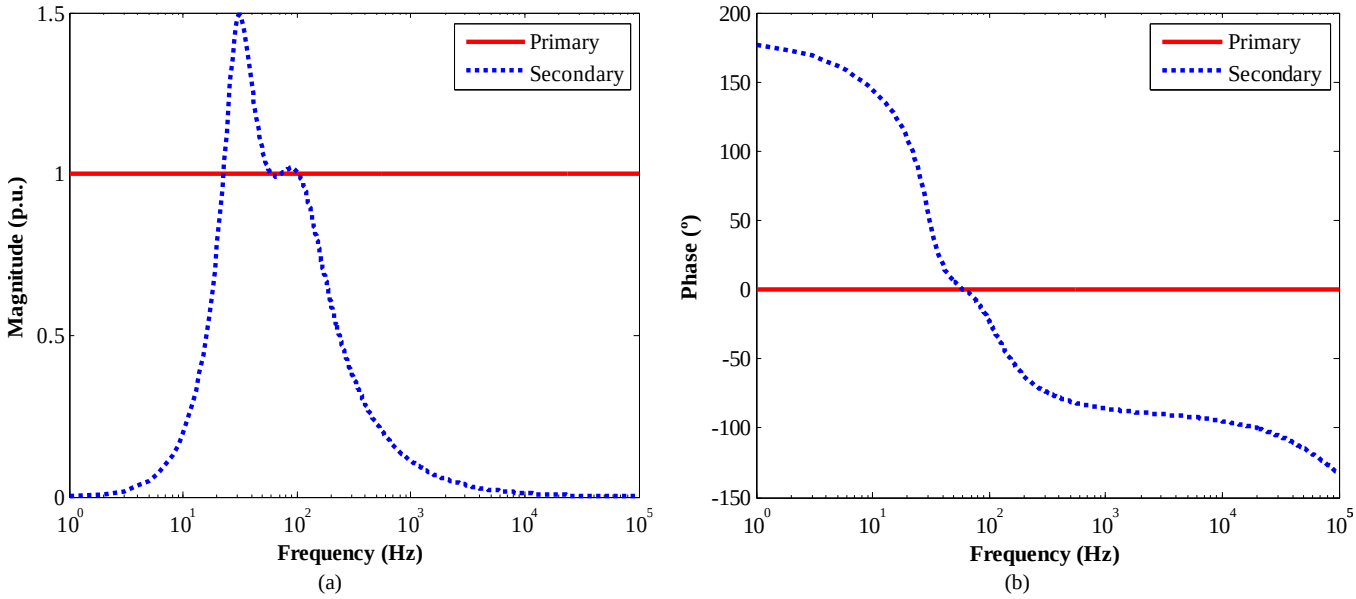

Fig. 4. CCVT 3 Frequency response: (a) Magnitude (p.u.); (b) phase (°).

In all analyzed CCVT models, it can be seen that at 60 Hz (power frequency) the secondary voltage is almost equal to the primary voltage (1 p.u.), presenting just a small phase angle. It indicates that the accuracy of the CCVT behavior during the steady-state is acceptable for most protection applications [6]. On the other hand, for any other frequency, the secondary voltage differs from the primary voltage. Thus, quick deviations on the primary voltage signal due to short-circuits are not properly followed by the CCVT secondary voltage signal, which may affect the protection and travelling wave-based fault location algorithms.

The CCVT 1 and CCVT 3 behavior attenuate high frequency components, as depicted in Figs. 2(a) and 4(a), respectively. In these cases, when only voltage measurements are available, the CCVT frequency response is cause for concern [3], since they can compromise the reliability of transient detection techniques, which are responsible for estimating the travelling waves' arrival time at the monitored power system buses [12].

On the other hand, the CCVT 2 dynamic behavior amplifies high frequency components far from the rated frequency, as demonstrated in Fig. 3(a). As shown later, this behavior may contribute to the improvement of the fault location estimation using travelling wave-based methods.

To illustrate in time domain the performance of the modeled CCVTs during fault-induced transients, primary and secondary voltages taken from CCVTs 1 and 2 during a phase-to-ground fault in a 230 kV power system are analyzed in Fig. 5. The same situation is carried out in a 500 kV power system to check the CCVT 3 performance, as well, as shown in Fig. 6. The ATP fault simulations were performed using the power systems described in section IV with a 5 μs time step.

It can be observed from Figs. 5 and 6 that CCVT 1 and CCVT 3 significantly attenuate the high frequency components on the secondary voltage waveform and cause relevant phase displacement at off-nominal frequencies as well. It happens due to CCVTs' frequency response, such as previously analyzed in Figs. 2 and 4. In these cases, the fault-induced transient detection required by the travelling wave-based fault locators can be compromised [5]. On the other hand, CCVT 2 amplifies the high frequency transient signals, as it can be seen in Fig. 3, facilitating the transient detection procedure.

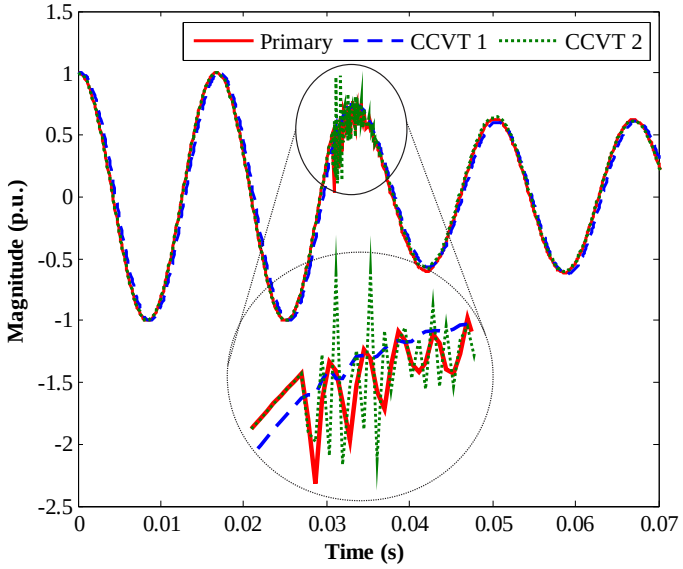

Fig. 5. CCVT 1 and CCVT 2 primary and secondary voltages signals during a fault.

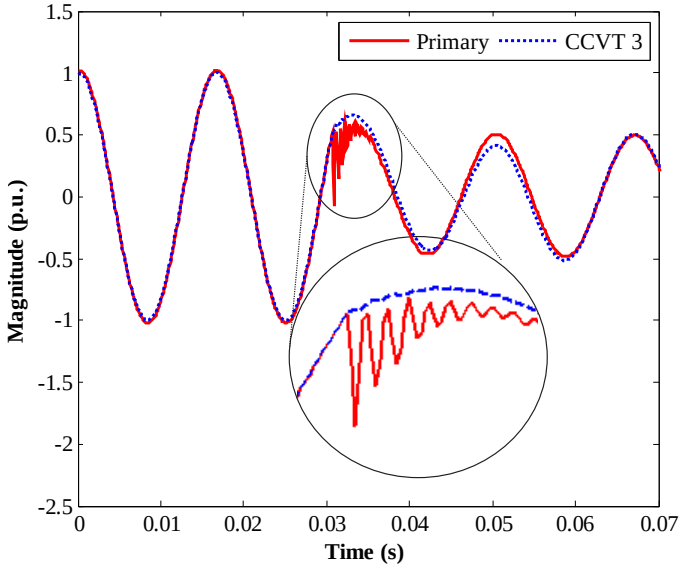

Fig. 6. CCVT 3 primary and secondary voltages signals during a fault.

III. Travelling Wave-Based Fault Locator

According to [13], two-terminal fault location methods are more reliable because they need to detect only the first incident travelling waves at both monitored terminals, even though the data synchronization from remote line ends is required. In this paper, the two-terminal travelling wave-based fault location method proposed in [13] is implemented. The basic principle of this technique consists in estimating the time difference between the first incident-travelling waves at both terminals. As shown in Fig. 7, the first incident-travelling waves are detected at t_{11} in bus 1, and at t_{21} in bus 2.

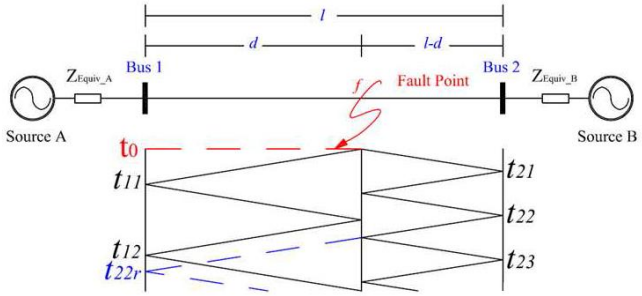

Fig. 7. Time-space diagram for a two-terminal monitored transmission line.

The estimated fault point $\tilde{d}$ from bus 1 is given by:

$$\tilde{d} = \frac{\ell + (t_{11} - t_{21})v}{2}, \quad (1)$$

where ℓ is the line length and v is the aerial mode travelling-wave propagation velocity, which is taken in this paper as:

$$v = \frac{1}{\sqrt{LC}}, \quad (2)$$

where L and C are the transmission line positive sequence inductance and capacitance per unit length, respectively.

Generally, the fault location estimation methods need two steps: 1) fault-induced transient detection and 2) fault distance estimation. The fault-induced transient detection methods used here are the ones reported in [7] and [8]. They are briefly described next.

A. Method proposed in [7]

This method is based on Park's Transformation (TDQ), which generates a rotating reference frame in synchronism with voltage and current phasors at power frequency. Thus, for an observer on the synchronous reference frame, the steady-state signal has negligible values whereas fault-induced transients assume large values enabling their identification.

Different from conventional high-speed detection algorithms, this method is also able to detect, in addition to fault-induced high frequency components, phase unbalance in three-phase signals, what makes it less affected by the CCVT frequency response.

B. Method proposed in [8]

This method is based on the maximal overlap discrete wavelet transform (MODWT), which is a variant of the discrete wavelet transform (DWT). It does not require the down-sampling process as the DWT does. In each simulation case, the MODWT wavelet coefficients are computed as soon as the sampling process is done. The fault-induced transient is detected through the analysis of the first scale wavelet coefficients since they are suitable for fast detection of the

highest frequency components [14].

According to [15], the wavelet Daubechies 4 (db4) provides an accurate detection of the fast transients in power systems, thereby it was used in this work.

During the steady-state, all wavelet coefficients are expected to be inside the range [μ-4σ, μ+4σ], where μ is the wavelet coefficient magnitude average and σ is the wavelet coefficient standard deviation. Therefore, during a fault situation, the wavelet coefficients go outside these thresholds, making the fault-induced transient detection possible.

C. Admissible error

The travelling wave-based fault location is directly influenced by the A/D converter sampling frequency and the maximum expected error is a function of the sampling rate. The fault-induced transient time is a multiple of the time step Δt used by the A/D converter. Therefore, some errors can arise in the fault location estimation due to hardware limitations. In this way, as reported in [12], the maximum admissible error is proportional to half time step, being estimated as:

$$|e| = \frac{\Delta t \cdot c}{2}, \tag{3}$$

where c is the speed of light.

Here, a sampling frequency of 20 kHz is used, so that the maximum admissible error is of about 7.5 km, in magnitude. Therefore, cases in which the estimated fault location error is above this value are classified as unsatisfactory cases, otherwise, they are classified as satisfactory cases.

IV. Simulation Studies and Analysis

Several ATP simulations of the 230 kV and 500 kV power systems presented in Fig. 7, both modeled with actual parameters, were performed using a 5 μs time step and assuming ℓ =200 km and ℓ =400 km. The power system and Thévenin equivalent parameters are shown in Tables II and III, respectively.

TABLE II
Transmission Line Parameters

Power System Voltage	Sequence	R (Ω/km)	X (Ω/km)	ωC (μ℧/km)
230 kV	Positive	0.098	0.510	3.252
	Zero	0.532	1.541	2.293
500 kV	Positive	0.0333	0.3170	5.2033
	Zero	0.3996	0.9921	3.0839

TABLE III
Parameters of the Thévenin Equivalents.

Power System Voltage	Source	V_{th} (p.u.)	Z_{th} (Z_{S1} e Z_{S2})			
			R_1 (Ω)	X_1 (Ω)	R_0 (Ω)	X_0 (Ω)
230 kV	S1	$1.02 \angle 0^o$	0.8713	25.661	1.0141	18.754
	S2	$0.98 \angle -10^o$	0.9681	28.513	1.1268	20.838
500 kV	S1	$1.00 \angle 0^o$	0.9681	28.513	1.1268	20.838
	S2	$0.99 \angle -10^o$	0.9681	28.513	1.1268	20.838

A total amount of 252 fault scenarios to each fault type was analyzed, resulting in 2520 fault scenarios. The simulation variables used to simulate the fault scenarios are shown in Table IV. After each simulation, the fault location is estimated using the transmission line primary voltage (V_{Pri}) and secondary voltage (V_{Sec}). The percentage errors are also computed for the cases in which the travelling wave-based fault locator uses as inputs the primary voltage (ε_{Pri}) and secondary voltage (ε_{Sec}) using:

$$\varepsilon_k = \frac{\left| d - \tilde{d}_k \right|}{\ell} \cdot 100, \tag{4}$$

where d and $\tilde{d}$ are the actual and estimated fault location, respectively, being $k = Pri$ or Sec.

TABLE IV
Simulation Variables Used to Simulate the Fault Scenarios.

Simulation variables	Values
Fault location (km)	20, 40, 60, 80, …, 140, 160, 180 (ℓ = 200 km)
	40, 80, 120, 160, …, 280, 320, 360 (ℓ = 400 km)
Fault type	AG, BG, CG, AB, BC, CA, ABG, BCG, CAG, ABC
Fault resistance (Ω)	1, 35, 70, 230
Inception angle (°)	0, 30, 60, 90, 120, 150, 180

The number of satisfactory and unsatisfactory fault point estimations using both fault-induced transient detection methods, for the modeled power systems with rated voltage of 230 kV and 500 kV, are shown in Tables V and VI, respectively.

TABLE V
Influence of CCVT on Travelling Wave-Based Fault Location to a 230 kV Power System.

ℓ	CCVT	Analyzed signal	NS*	TDQ*		MODWT*	
				UE	SE (%)	UE	SE (%)
200	CCVT 1	V_{Pri}	2520	4	99.84	0	100
		V_{Sec}	2520	40	98.41	64	97.46
	CCVT 2	V_{Pri}	2520	4	99.84	0	100
		V_{Sec}	2520	3	99.88	0	100
400	CCVT 1	V_{Pri}	2520	0	100	0	100
		V_{Sec}	2520	0	100	32	98.73
	CCVT 2	V_{Pri}	2520	0	100	0	100
		V_{Sec}	2520	0	100	0	100

*where: UE = Unsatisfactory estimation; SE = Satisfactory estimation and NS = number of simulations.

TABLE VI
INFLUENCE OF CCVT ON TRAVELLING WAVE-BASED FAULT LOCATION TO A 500 KV POWER SYSTEM.

ℓ	CCVT	Analyzed signal	NS*	TDQ*		MODWT*	
				UE	SE (%)	UE	SE (%)
200	CCVT 3	V_{Pri}	2520	0	100	0	100
		V_{Sec}	2520	10	99.6	180	92.86
400	CCVT 3	V_{Pri}	2520	0	100	0	100
		V_{Sec}	2520	0	100	188	92.54

*where: UE = Unsatisfactory estimation; SE = Satisfactory estimation and NS = number of simulations.

The calculated percentage errors ε_{Pri} and ε_{Sec} are presented as boxplots, which consist in a type of plot able to visually reveal some basic statistics of a data set, using five thresholds: the maximum value, represented by the upper whisker; the upper quartile, represented by the upper boundary of the box; the median quartile, represented by the intermediate line inside the box; the lower quartile, represented by the lower boundary of the box; and the minimum value, represented by the lower whisker. The upper quartile, the median and the lower quartile represent the maximum fault location error in 75%, 50% and 25% of the simulated fault cases, respectively. The obtained boxplots are shown in Fig. 8 to a 230 kV analysis and in Fig 9. to a 500 kV analysis. In order to make some comparative analysis about the influence of the CCVT on travelling wave-based fault location methods, the average errors and standard deviations obtained for each analyzed transient detection methods are presented in Tables VII and VIII.

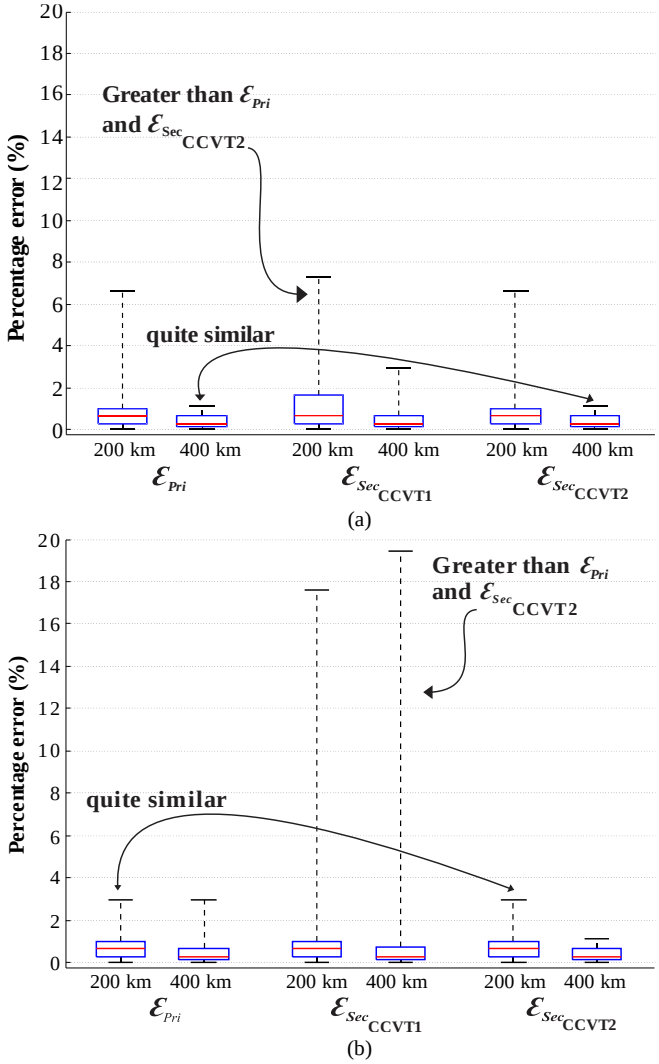

Fig. 8. Boxplots representing statistics errors in fault location estimation in the 230 kV power system when the fault-induced transient is detected using: (a) TDQ; (b) MODWT.

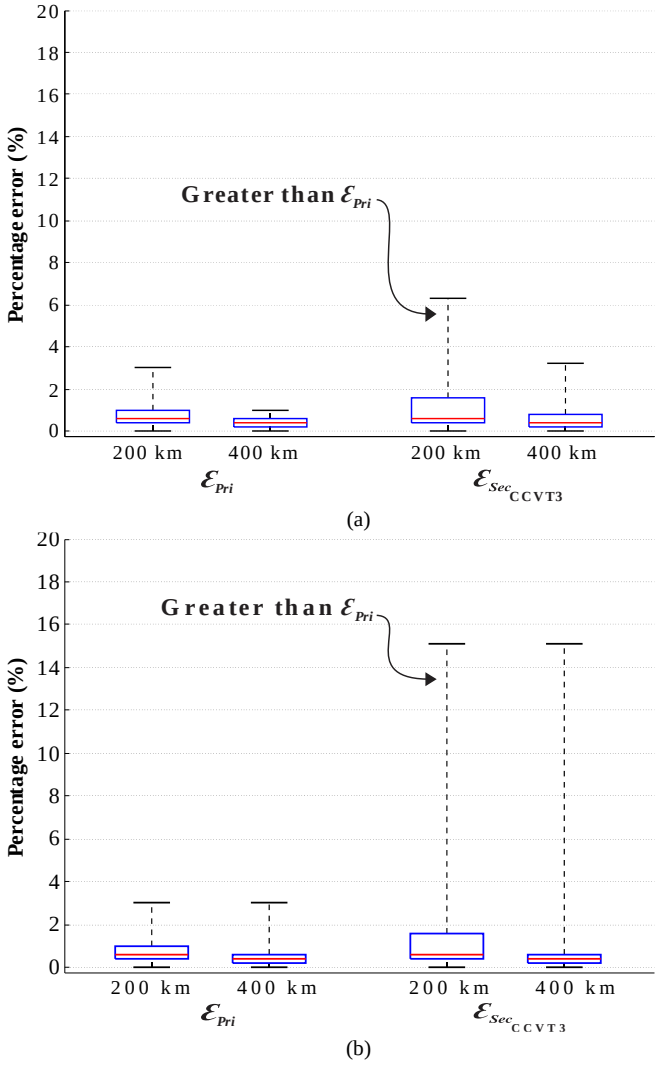

Fig. 9. Boxplots representing statistics errors in fault location estimation in the 500 kV power system when the fault-induced transient is detected using: (a) TDQ; (b) MODWT.

TABLE VII
FAULT LOCATION ESTIMATED AVERAGE ERRORS AND STANDARD DEVIATION TO A 230 KV POWER SYSTEM.

Transient detection method	ℓ	Analyzed signal	Average error	Standard deviation
TDQ	200	ε_{Pri}	0.824%	0.606%
		$\varepsilon_{SecCCVT1}$	0.952%	0.872%
		$\varepsilon_{SecCCVT2}$	0.823%	0.599%
	400	ε_{Pri}	0.472%	0.356%
		$\varepsilon_{SecCCVT1}$	0.482%	0.373%
		$\varepsilon_{SecCCVT2}$	0.470%	0.355%
MODWT	200	ε_{Pri}	0.836%	0.598%
		$\varepsilon_{SecCCVT1}$	1.001%	1.316%
		$\varepsilon_{SecCCVT2}$	0.833%	0.593%
	400	ε_{Pri}	0.476%	0.370%
		$\varepsilon_{SecCCVT1}$	0.595%	1.292%
		$\varepsilon_{SecCCVT2}$	0.473%	0.357%

TABLE VIII
FAULT LOCATION ESTIMATED AVERAGE ERRORS AND STANDARD DEVIATION TO A 500 KV POWER SYSTEM.

Transient detection method	ℓ	Analyzed signal	Average error	Standard deviation
TDQ	200	ε_{Pri}	0.817%	0.530%
		$\varepsilon_{SecCCVT3}$	0.899%	0.685%
	400	ε_{Pri}	0.497%	0.336%
		$\varepsilon_{SecCCVT3}$	0.555%	0.462%
MODWT	200	ε_{Pri}	0.828%	0.551%
		$\varepsilon_{SecCCVT3}$	0.977%	1.306%
	400	ε_{Pri}	0.503%	0.351%
		$\varepsilon_{SecCCVT3}$	0.564%	1.027%

In the 230 kV power system with CCVT 1, the MODWT did not detect the fault-induced transient in 5 simulation cases. This number increased to 10 cases for the 400 km line in the same power system. In the 500 kV power system with CCVT 3, the MODWT did not detect the fault-induced transient in 158 cases, for the 200 km line, and in 162 simulation cases, for the 400 km line.

In general, taking the unsatisfactory estimations shown in Tables V and VI, one can notice that the TDQ and MODWT performances were more compromised when the CCVT 1 and CCVT 3 secondary voltages were used as inputs of the fault location algorithm. In fact, the CCVT 1 and CCVT 3 dynamic behavior significantly attenuate high frequency components on the secondary voltage waveform (Figs. 2 and 4). In addition, the average errors and standard deviations of the fault point estimation also increased when compared to the results obtained from primary voltage, which represents the reference signal, as shown in Tables VII and VIII. In these cases, when only voltage measurements are available, the CCVT frequency response can compromise the transient detection techniques reliability. However, the TDQ-based transient detection algorithm is less affected by the CCVT 1 and CCVT 3 frequency responses than the MODWT-based transient detection method, since it detects imbalances as well. On the other hand, the TDQ and MODWT performances were slightly improved when the CCVT 2 secondary voltage was taken as the fault location algorithm input. The obtained average errors and standard deviation presented in Table VII are smaller than case when the primary voltage is taken as input to the fault location algorithm. In fact, as shown in Fig. 3, the CCVT 2 frequency response amplifies high frequency components on the secondary voltage waveform which makes the fault-induced transient detection procedure easier, improving the travelling wave-based fault locator performance.

From the boxplots shown in Figs. 8 and 9, analyzing the maximum errors, one can notice that the TDQ-based transient detection algorithm is less affected by the CCVT frequency responses than the MODWT-based transient detection method. Also, one can see that the obtained errors, when using the CCVT 2, are quite similar to those when the primary voltage is considered.

According to the results presented in Tables V and VI, the number of unsatisfactory fault point estimations decreased when the line length increased. This fact can be explained due to the System Impedance Ratio (SIR), which is crucial in the CCVT secondary voltage behavior during fault conditions. The SIR consists in the relation between the Thévenin equivalent source impedance at the monitored bus and the transmission line impedance [16]. In order to make some analysis, consider electrical power system presented in Fig. 7, which is submitted to a three-phase short-circuit at *d* km far away from the monitored bus 1. In this situation, the bus 1 voltage $\hat{V}_{Bus1}$ is computed using:

$$\hat{V}_{Bus1} = E_{th1}\frac{d \cdot Z_{L1}}{Z_{th1} + d \cdot Z_{L1}}, \tag{5}$$

Normalizing (5) by the transmission line impedance ℓZ_{L1}, one can obtain:

$$\hat{V}_{Bus1} = E_{th1}\frac{\frac{d}{\ell}}{\frac{Z_{th1}}{\ell Z_{L1}} + \frac{d}{\ell}} = E_{th1}\frac{d_{pu}}{SIR + d_{pu}} = \frac{E_{th1}}{\frac{SIR}{d_{pu}} + 1}, \tag{6}$$

The voltage at the monitored terminal is a superposition of the source voltage connected to the bus and the harmonic

frequency components due to the CCVT dynamic behavior. According to (6), the greater the SIR, the lower the voltage at the monitored terminal, making the CCVT influence more evident. Therefore, as soon as the line length increases, the SIR decreases and the CCVT effect is less evident.

V. Conclusions

In this paper, the influence of two 230 kV and one 500 kV CCVTs available in the literature on a two-terminal travelling wave-based fault location method was analyzed. A large amount of fault simulations were performed in a 230 kV and 500 kV power systems, both modeled with actual parameters using the ATP software. In each simulation case, the fault location, fault resistance, fault type and inception angle were varied and the fault point was estimated taking the primary voltage (which represents the reference signal) and secondary voltage as inputs of the fault location algorithm.

From the obtained results, the estimated fault locations are directly affected by CCVT dynamic behavior. In cases which the CCVT frequency response significantly attenuate the high frequency components on the secondary voltage waveform, the fault-induced transient detection method performance can be compromised. On the other hand, in cases in which the CCVT frequency response amplifies high frequency components, the fault-induced transient detection algorithm performance can be improved. This fact is in contrast with those reported in several references in this area, which state that the CCVT always affect travelling wave-based methods. Besides, the obtained results show the CCVT transient behavior can be more evident depending on how big the SIR of the power system is, highlighting the need to consider it during the evaluation of travelling wave-based approaches.

VI. Acknowledgment

The authors gratefully acknowledge the reviewers for the invaluable suggestions.

VII. References

[1] B. Kasztenny, D. Sharples, V. Asaro, and M. Pozzuoli, “Distance Relays and Capacitive Voltage Transformers-Balancing Speed and Transient Overreach”. In: Annual Conference for Protective Relay Enginners. College Station Texas, v. 53, 2000.

[2] C. A. Silva, D. Fernandes Jr. and W. L. A. Neves, “Correction of the Secondary Voltage of Coupling Capacitor Voltage Transformers in Real Time,” International Conference on Power Systems Transients 2011 – IPST 2011, Delft – The Netherlands, June 2011.

[3] M. M. Saha, J. Izykowski, and E. Rosolowski, “Fault Location on Power Networks,” ser. Power Systems. London: Ed. Springer, 2010.

[4] D. Hou and J. Roberts, “Capacitive voltage transformer: transient overreach concerns and solutions for distance relaying,” in Canadian Conference on Electrical and Computer Engineering, vol. 1, 1996.

[5] R. G. Bainy, F. V. Lopes, W. L. A. Neves, “Benefits of CCVT Secondary Voltage Compensation on Travelling Wave-Based Fault Locators”, IEEE Power & Energy Society General Meeting 2014, Washington, USA, July 2014.

[6] E. Pajuelo, G. Ramakrishna, M. S. Sachdev, “Phasor Estimation Technique to Reduce the Impact of Coupling Capacitor Voltage Transformer Transientes”, University of Saskatchewan, Canada, August, 2006.

[7] F. V. Lopes, D. Fernandes Jr., and W. L. A. Neves, “Transients detection in EHV trasmission lines using Park’s transformation,” in *2012 IEEE PES Transmission and Distribution Conference and Exposition*, 2012.

[8] F. B. Costa and B. A. Souza, “Fault-induced transient analysis for real-time fault detection and location in transmission lines”, International Conference on Power Systems Transients 2011 – IPST 2011, Delft – The Netherlands, June 2011.

[9] IEEE Power System Relaying Committee. (2004). EMTP Reference Models for Transmission Line Relay Testing. [S.l.]. Available in: <http://www.pes-psrc.org>.

[10] A. V. Carvalho Jr. (2008). Interação Transitória entre Transformadores de Potencial Capacitivos e Linhas de Transmissão: Uma Contribuição para Minimizar Falhas. Master thesis in portuguese, Federal University of Pernambuco.

[11] *“ATP-Alternative Transient Program–Rule Book,”* Leuven EMTP Center, Herverlee, Belgium, 1987.

[12] F. V. Lopes, D. Fernandes Jr., and W. L. A. Neves, “Fault location on transmission lines based on travelling waves,” *International Conference on Power Systems Transients*, June 2011.

[13] P. F. Gale, P. A. Crossley, Xu Bingyin, Ge Yaozhong, B. J. Cory, J. R. J. Barker, "Fault Location Based on Travelling Waves," *Fifth International Conference on Developments in Power System Protection*, pp. 54-59, 1993.

[14] F. Costa, B. Souza, and N. Brito, “A wavelet-based algorithm to analyze oscillographic data with single and multiple disturbances,” in *2008 IEEE Power and Energy Society General Meeting – Convention and Delivery of Electrical Energy in the 21st Century*, july 2008, pp. 1 – 8.

[15] M. H. J. Bollen and I. Y.-H. Gu. *Signal Processing of Power Quality Disturbances*. New York, USA: IEEE, 2006.

[16] The Institution of Engineering and Technology, *Power System Protection 2: Systems and Methods*, vol. 2, Ed. London: The Electricity Training Association, 1995.